Effects of Oxygen Concentration on the Reaction to Fire of Cross-Laminated Timber in a Controlled-Atmosphere Cone Calorimeter

Véronique Marchetti, Gaelle Fontaine, Adèle Lamandé, Serge Bourbigot

Metadata of the article that will be visualized in OnlineFirst

ArticleTitle	Effects of Oxygen Concentration on the Reaction to Fire of Cross-Laminated Timber in a Controlled-Atmosphere Cone Calorimeter	
Article Sub-Title		
Article CopyRight	Springer Science+Business Media, LLC, part of Springer Nature (This will be the copyright line in the final PDF)	
Journal Name	Fire Technology	

Corresponding Author	FamilyName	**Marchetti**
	Particle	
	Given Name	**Véronique**
	Suffix	
	Division	
	Organization	Centre Scientifique et Technique du Bâtiment (CSTB), University of Paris-Est
	Address	Champs-sur-Marne, France
	Phone	
	Fax	
	Email	veronique.marchetti@cstb.fr
	URL	
	ORCID	
Corresponding Author	FamilyName	**Fontaine**
	Particle	
	Given Name	**Gaëlle**
	Suffix	
	Division	
	Organization	CNRS, INRAE, Centrale Lille, UMR 8207 - UMET - Unité Matériaux et Transformations, University of Lille
	Address	59000, Lille, France
	Phone	
	Fax	
	Email	gaelle.fontaine@centralelille.fr
	URL	
	ORCID	http://orcid.org/0000-0002-7113-1687
Author	FamilyName	**Lamandé**
	Particle	
	Given Name	**Adèle**
	Suffix	
	Division	
	Organization	Centre Scientifique et Technique du Bâtiment (CSTB), University of Paris-Est
	Address	Champs-sur-Marne, France
	Division	
	Organization	CNRS, INRAE, Centrale Lille, UMR 8207 - UMET - Unité Matériaux et Transformations, University of Lille
	Address	59000, Lille, France
	Phone	
	Fax	
	Email	
	URL	
	ORCID	

Author	FamilyName	**Bourbigot**
	Particle	
	Given Name	**Serge**
	Suffix	
	Division	
	Organization	CNRS, INRAE, Centrale Lille, UMR 8207 - UMET - Unité Matériaux et Transformations, University of Lille
	Address	59000, Lille, France
	Division	
	Organization	Institut Universitaire de France (IUF)
	Address	Paris, France
	Phone	
	Fax	
	Email	
	URL	
	ORCID	

Abstract	This paper deals with the fire reaction as well as the gas and aerosol production of Cross-Laminated Timber (CLT) submitted to fire in oxygen-depleted environments. A Controlled-Atmosphere Cone Calorimeter (CACC) coupled to a Fourier Transform Infrared (FTIR) spectrometer and an Electrical Low Pressure Impactor (ELPI) was used for this purpose. This combination enabled simultaneous assessments of Mass Loss Rate (MLR), evolved gases (qualitatively and quantitatively) and aerosols (size distribution and concentration) in the smoke. Several oxygen levels (21, 18, 15 and 10% O_2) were studied at an external heat flux of 50 and 20 kW/m2. The combination of these two parameters allowed the response of CLT to be classified according to different fire scenarios. Indeed, an oxygen decrease shifted the combustion towards incompleteness or even prevented combustion. The production of carbon monoxide and methane was significantly promoted as well as acetaldehyde and ethene in some cases. The aerosol size distribution was slightly affected by oxygen depletion. Furthermore, decreasing the heat flux greatly reduced the decomposition rate but also promoted the production of unburnt gases.

Keywords (separated by '-')	Cross-laminated timber - Controlled-atmosphere cone calorimeter - Oxygen vitiation - Gases - Aerosols

Footnote Information	

Effects of Oxygen Concentration on the Reaction to Fire of Cross-Laminated Timber in a Controlled-Atmosphere Cone Calorimeter

Adèle Lamandé, *Centre Scientifique et Technique du Bâtiment (CSTB),*
University of Paris-Est, Champs-sur-Marne, France; CNRS, INRAE,
Centrale Lille, UMR 8207 - UMET - Unité Matériaux et Transformations,
University of Lille, 59000 Lille, France

Véronique Marchetti*, *Centre Scientifique et Technique du Bâtiment (CSTB),*
University of Paris-Est, Champs-sur-Marne, France

Serge Bourbigot, *CNRS, INRAE, Centrale Lille, UMR 8207 - UMET - Unité*
Matériaux et Transformations, University of Lille, 59000 Lille, France;
Institut Universitaire de France (IUF), Paris, France

Gaëlle Fontaine ⓘ*, *CNRS, INRAE, Centrale Lille, UMR 8207 - UMET -*
Unité Matériaux et Transformations, University of Lille, 59000 Lille,
France

Abstract. This paper deals with the fire reaction as well as the gas and aerosol production of Cross-Laminated Timber (CLT) submitted to fire in oxygen-depleted environments. A Controlled-Atmosphere Cone Calorimeter (CACC) coupled to a Fourier Transform Infrared (FTIR) spectrometer and an Electrical Low Pressure Impactor (ELPI) was used for this purpose. This combination enabled simultaneous assessments of Mass Loss Rate (MLR), evolved gases (qualitatively and quantitatively) and aerosols (size distribution and concentration) in the smoke. Several oxygen levels (21, 18, 15 and 10% O_2) were studied at an external heat flux of 50 and 20 kW/m². The combination of these two parameters allowed the response of CLT to be classified according to different fire scenarios. Indeed, an oxygen decrease shifted the combustion towards incompleteness or even prevented combustion. The production of carbon monoxide and methane was significantly promoted as well as acetaldehyde and ethene in some cases. The aerosol size distribution was slightly affected by oxygen depletion. Furthermore, decreasing the heat flux greatly reduced the decomposition rate but also promoted the production of unburnt gases.

---

* Correspondence should be addressed to: Véronique Marchetti, E-mail: veronique.marchetti@cstb.fr; Gaëlle Fontaine, E-mail: gaelle.fontaine@centralelille.fr

1. Introduction

In recent years, there has been a great deal of interest in sustainable construction, with the objective of developing energy-efficient buildings with a low carbon footprint. To fulfill this objective, renewable and/or recycled construction materials are increasingly used, as wood-based materials. In the building field, Cross-Laminated Timber (CLT) is widely used because of its structural properties. With low weight and fast construction times, CLT challenges the use of traditional dense materials like steel and concrete. However, like most organic-based materials, CLT decomposes when exposed to fire. Thus, it is important to study its behavior under different fire scenarios to implement suitable protection methods to ensure the safety of people. Especially, knowledge of gas and aerosol emissions from the thermal decomposition of CLT is paramount. Indeed, during a building fire, most deaths are due to smoke release [1]. Smoke reduces visibility, causes impaired vision and respiratory problems due to irritating and asphyxiating gases. Consequently, this leads to impairment of escape and increases the time to escape and the probability of injuries or death [2]. To ensure safe evacuation, the standard ISO 13571 [3] subdivides the risks to people escaping a fire into the effects of heat, asphyxiant and irritant gases and visual obscuration by smoke. Each component is assessed separately and untenability is defined when one of the components reaches a level that prevents escape. This underlines the need to assess the toxicity of materials to have a better understanding of phenomena occurring during a fire and to improve fire safety engineering. Toxicants production and yield depend on the material composition and the fire conditions including oxygen concentration and temperature. An under-ventilated or low oxygen level (vitiated) atmosphere increases the production of dangerous gases for humans. Indeed, the oxygen level quickly decreases until it no longer allows complete combustion. A dense, carbon monoxide (CO) rich smoke as well as other toxic gases and non-toxic gases are produced. A complete assessment of the thermal decomposition of materials with gaseous emissions and aerosols production is crucial for fire safety.

To date, there are many bench-scale devices available but there is no international agreement or standard on how to assess this toxicity. The main challenges are to correlate results with real scale as well as to simulate and control different fire scenarios. The Controlled-Atmosphere Cone Calorimeter (CACC) is a modified design from the Cone Calorimeter developed by V. Babrauskas and standardized in ISO 5660–1 [4]. The standard cone calorimeter is widely used to assess the reaction to fire of a material but as its design is open, it represents well-ventilated conditions and it does not enable reduced oxygen atmospheres. Consequently, research focused on the development of enclosed cone calorimeters where the oxygen level of the atmosphere can be controlled. Werrel categorized them into two designs: closed designs and open designs [5]. These latter have no connection between the exhaust hood and the enclosure. Several open designs were set up to study the reaction to fire of various materials, *e.g.* polymethylmethacrylate (PMMA) [5–10], polyethylene (PE) [7, 11], polyisocyanurate (PUR) [12], acrylonitrile butadiene styrene (ABS) [7, 13], polyvinyl chloride (PVC) [10, 14], sandwich

85 material [15] or wood [16]. As there was no international agreement on the CACC
86 design nor the experimental protocol, Marquis et al. [6] investigated the interpre-
87 tation and accuracy of results with different setup. They observed that the design
88 of the combustion enclosure may affect the material burning behavior and the
89 accuracy of measurement. Therefore, they suggested constructing a chimney
90 between the enclosure and the exhaust hood to reduce the post-oxidation phe-
91 nomenon. From this work, the CACC and the experimental protocol associated
92 are now standardized with ISO 5660–5:2020 [17]. In this standard, new equations
93 developed by Werrel et al. [5] to calculate the Heat Release Rate (HRR) are pre-
94 sented. Indeed, the exhaust gases are diluted by excess air drawn from the labora-
95 tory surroundings. The heat-induced changes in the dilution ratio affect the
96 measurement of the oxygen and the calculation of the HRR. The error in the
97 HRR calculation increases at a significant order of magnitude ($\approx$ 30%) when the
98 oxygen content in the enclosure is decreased below 18 vol % [5]. Thus, Werrel
99 et al. [5] considered the variations in the flow rate of the ambient air from the lab-
100 oratory drawn into the exhaust hood to avoid inaccurate HRR calculations.

101 Work done on several CACC designs and materials has shown trends in the
102 effect of oxygen. Indeed, the HRR [7, 8] and the Mass Loss Rate (MLR) [7, 8, 18]
103 decrease when oxygen concentration decreases (vitiation). On the contrary, the
104 carbon monoxide production [7, 19] increases with vitiation whereas the time to
105 ignition remain unchanged [8]. However, the effect of oxygen on the fire behavior
106 of CLT in a CACC has never been studied. More specifically, there is a lack of
107 data on the gaseous emissions and the aerosols production of CLT in vitiated
108 environments.

109 This paper depicts the results of the effects of oxygen concentration on the reac-
110 tion to fire and gas and aerosol production of CLT in a CACC. To have a better
111 understanding of the complex phenomena occurring, a homemade bench is
112 designed where a Fourier Transform Infrared (FTIR) spectrometer as well as an
113 Electrical Low Pressure Impactor (ELPI) are coupled to the CACC. Particularly,
114 the samplings for FTIR and ELPI analysis are made in the chimney instead of in
115 the exhaust duct in order to limit the loss of species due to dilution/oxidation with
116 ambient air. The experiments are realized at an irradiance of 50 and 20 kW/m^2 to
117 assess the fire risks of CLT under different fire scenarios, respectively well-venti-
118 lated fires and smoldering.

2. Material and Method

2.1. *Material*

121 The material used in this study is a commercial Cross-Laminated Timber (CLT)
122 made from spruce. The panels used consist of two 20 mm thick plies glued per-
123 pendicular to each other. The glue used is polyurethane based and it does not
124 release formaldehyde. The sample dimensions are 100 mm long, 100 mm wide and
125 40 mm thick. It has a specific gravity of 500 kg/m^3, a thermal conductivity of 0.12
126 W/m.K and a heat capacity of 1600 J/kg K (Table 1).

Table 1
CLT Properties Given by the Manufacturer

Specific gravity	500 kg/m³
Thermal conductivity	0.12 W/m K
Heat capacity	1600 J/kg K

127   The specimens are conditioned at 23 ± 2 ℃ and at a relative humidity of $50 \pm$
128 5% until the mass is constant, in order to reach a moisture of wood close to 11%
129 as described in the standard EN 13238 [20].

2.2. Controlled-Atmosphere Cone Calorimeter

131 Very recently an experimental standard was released, it is entitled "ISO 5660–5:
132 Heat release rate (cone calorimeter method) and smoke production rate (dynamic
133 measurement) under reduced oxygen atmospheres" [17]. It specifies how to use the
134 cone calorimeter to perform tests in controlled atmospheres. The device is able to
135 work under 1% to 21% of oxygen and to deliver between 10 and 180 L/min of
136 gas. The enclosure, described in Figure 1, is a stainless-steel box of 37 30 30 cm³ in
137 dimensions with the standard cone heater on top, a door and a window. Inside,
138 there is a load cell and two gas inlet ports. The atmosphere is adjusted by control
139 of the volume flow rate of air and nitrogen, each with a rotameter and monitored
140 by an additional oxygen analyzer that is linked to the enclosure. Moreover, to
141 avoid excessive heating and radiation of the system, a cooling ring is set between
142 the cone heater and the top of the enclosure as well as a cooling hood on the load
143 cell and a cooling serpentine around the load cell's rod.
144   The experimental method is similar to that of the standard cone calorimeter.
145 The surface area of the sample is 100 100 mm². The sample can be exposed to a
146 constant irradiance level up to 100 kW/m². Above the sample, a spark plug ignites
147 the flammable gases that might be released. These gases are then collected in the
148 exhaust hood and send through a duct provided with thermocouples, pressure sen-
149 sor, smoke measurement and a ring probe for O_2, CO and CO_2 analyzers. As a
150 result, heat release rate, mass loss rate, smoke density and gas concentration are
151 assessed.
152   A drawback of the CACC is the possible post-oxidation of the fire effluent
153 between the enclosure and the exhaust sampling point that would modify HRR
154 and gas measurements. To overcome this issue, the standard specifies to set a
155 chimney of 60 cm long and of 11.5 cm in diameter above the cone heater. It can
156 be made of metal or of quartz; the differences have been discussed in [6].
157   In this study, the CACC depicted above is used but with some modifications.
158 Indeed, to avoid heat losses, the four walls of the enclosure are insulated with
159 25 mm calcium silicate panels. Moreover, a new metallic chimney is set to ensure
160 better sampling of effluents.

Effects of Oxygen Concentration on the Reaction to Fire of Cross-Laminated Timber
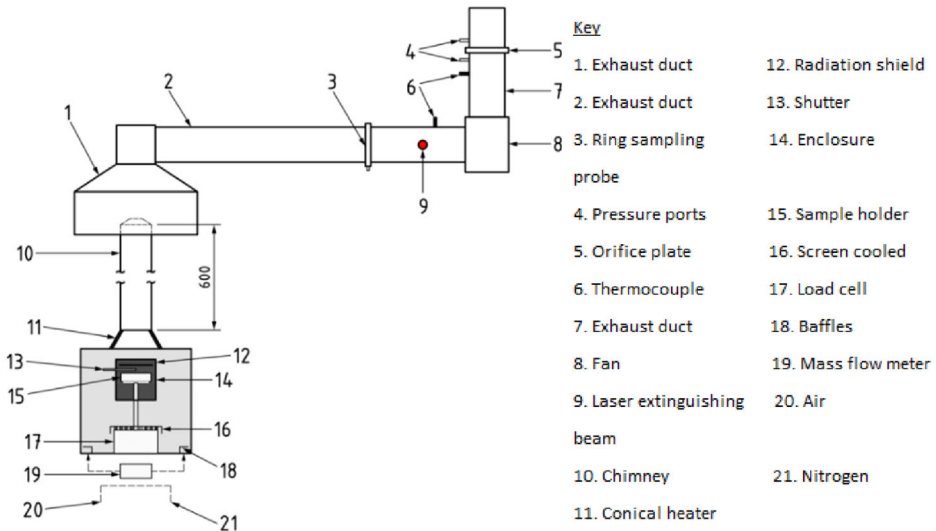
**Figure 1.** CACC design from ISO 5660–5 [16].

2.3. Controlled-Atmosphere Cone Calorimeter Coupled with FTIR and ELPI

To study the influence of oxygen concentration on the gas production and the aerosol size distribution, two devices were respectively coupled to the CACC: a Fourier Transform Infrared spectrometer and an Electrical Low Pressure Impactor. Instead of classical sampling in the duct, the raw sampling method is used in this study. It was recently developed in order to avoid the loss of effluent when assessing its composition. Indeed, the effluents can condensate while being transported and more importantly when diluted species are lost due to their low concentration (acrolein or formaldehyde for example). Dilution lowers the dew point of the sample so that the water vapor in the effluents does not condense when the sample is cooled by dilution [21]. Consequently, the sampling of the effluent is made in the chimney instead of in the exhaust duct. Further details on the sampling method can be found in literature [10, 12, 21, 22].

In this study, a new metallic chimney (Figure 2a), was designed in order to insert a sampling probe for the FTIR and another one for the ELPI. The chimney is 60 cm long and of 11.5 cm in diameter with its top diameter reduced to 5 cm to assure a sufficient velocity flow of the smoke in the duct. The FTIR sampling probe (Figure 2b) is located near the outlet of the cone and is composed of two flute probes of four holes each to have a homogenous mixture. The holes face away the stream of effluent. The ELPI measurement consists in a single point probe that ensures isokinetic sampling.

An Antaris IGS FTIR spectrometer equipped with a nitrogen Mercury Cadmium Telluride (MCT) detector, 0.2L volume gas cell, and a 2 m optical path length is set. Each scan was taken at 1.76 s and 0.5 cm^{-1} as spectral resolution. At the output of the chimney, the gases are transported through a PTFE line. The
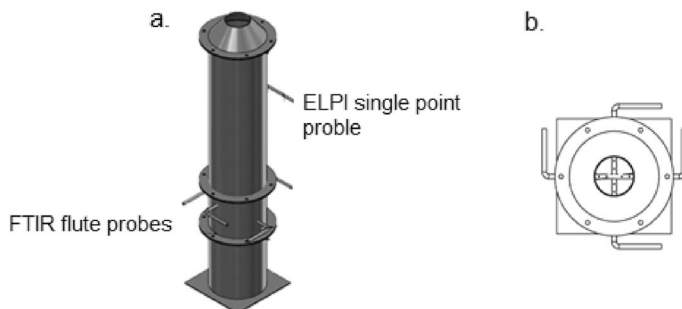
Figure 2. **(a) designed metallic chimney for raw sampling; (b) top view of FTIR probes.**

186 FTIR gas cell as well as the PTFE gas transport line are heated at 180 ℃ to avoid
187 condensation. In the end, gases are cooled down, dried, filtered and then evacu-
188 ated with a membrane pump. The gas cell was kept at a constant pressure of
189 650 Torr with a pressure gauge with regulating valve. Each gas (CO_2, CO, H_2O,
190 CH_4, CH_2O, C_2H_4O, C_2H_4, C_3H_6) is calibrated using the Classical Least Square
191 (CLS) algorithm. For each gas, a dilution range was analyzed with the FTIR.
192 Characteristic peaks on FTIR spectra were carefully selected by considering all the
193 unavoidable interferences between substances [23].
194   ELPIs are cascade impactors widely used to measure in real-time the particle
195 size distribution and the concentration of aerosols. An ELPI as well as two
196 diluters from Dekati are set. The ELPI principle consists of three main steps.
197 First, the sampled aerosols are subjected to a unipolar positive ion environment in
198 a corona charger where they are electrically charged. Then, the charged particles
199 enter a low-pressure cascade impactor where they are classified into size of 7 nm
200 to 10 m according to their aerodynamic diameter which determines their deposi-
201 tion at a particular ELPI stage. Finally, the charges carried by the aerosols are
202 continuously measured at each impactor stage by sensitive electrometers. The
203 measured current values are converted to give a number of particles by cm^3 using
204 transfer functions provided by manufacturers. The transport line is an antistatic
205 PTFE pipe heated at 180℃ to avoid effects of condensed humidity on the mea-
206 surement. A vacuum pump is set to ensure an isokinetic sampling flow at a rate of
207 10 L/min. Double dilution of the effluents is set upstream the ELPI particle sizer
208 with two diluters DI-1000 from Dekati. The first one is heated at 2000℃ to avoid
209 loss in aerosol concentration while the second one prevents nucleation of the aero-
210 sols. The diluters are set in series to provide a ratio of dilution of 83.

2.4. Experimental Procedure

212 Samples are tested in the horizontal orientation. The sample holder is used with a
213 frame to reduce the exposed surface of the sample. A 64 kg/m^3 ceramic fiber insu-
214 lation pad is put on the backside of the sample as specified in the ISO 5660–1
215 standard [4]. The volumetric flow rate of extraction through the exhaust duct of

Effects of Oxygen Concentration on the Reaction to Fire of Cross-Laminated Timber

216 the calorimeter is set at 24 ± 2 L/s at 23 ℃. The inlet volume flow rate is set at
217 150 ± 5 L/min at 23 ℃. Tests are carried out at 50 and 20 kW/m² and at 21, 18,
218 15 and 10 vol% of oxygen respectively. All tests are performed at least three times
219 and the curve presented represents a single specimen that best fits the mean curve.
220 Data were collected with a 1 s sampling interval for the cone measurement, 1 s for
221 the ELPI and 1.76 s for the FTIR.

3. Results and Discussion

223 The reaction to fire of Cross-Laminated Timber is strongly dependent on the envi-
224 ronment conditions such as the oxygen level and the heat flux. The combustion is
225 considered incomplete when the CO/CO_2 ratio is greater than 0.05 [25]. For the
226 whole study, the time to ignition is defined as t_i, the time to flameout as t_f, the
227 peak of HRR as pHRR and the peak of MLR as pMLR.

3.1. Influence of Oxygen Level at 50 kW/m²

229 *3.1.1. Mass Loss and Heat Release 3.1.1.1. Mass Loss* The influence of oxygen
230 level on the remaining mass and the mass loss rate at 50 kW/m² was first studied
231 (Figure 3. The decomposition process of CLT at 21 vol% O_2 is first described
232 before studying the effect of oxygen.
233   The decomposition pathway of CLT at 21 vol% O_2 is assessed via the mass loss
234 (Figure 3b). First, between 0 and 19 s, as the temperature at the surface of CLT
235 increases, the sample starts to degrade. The free water contained in wood (around
236 11%) evaporates. Simultaneously, the chemical bonds of wood polymer chains
237 (cellulose, hemicellulose and lignin) start to break [26, 27]. Consequently, tars and
238 decomposition gases are produced. As the gases leave the solid, they encounter the
239 oxygen present in the atmosphere. Concurrently, oxygen may diffuse into the solid
240 and oxidize the wood effluents. Triggered by the igniter, the mixture ignites and
241 the flame spreads onto the whole surface of the sample. It results, in a second
242 step, in a fast increase of the MLR, which reaches a maximum at 60 s. A car-
243 bonaceous layer is formed on top of the wood, which reduces the heat transfers
244 between the wood surface and the pyrolysis front. This carbonaceous layer creates
245 then a thermal insulation [28]. As a result, pyrolysis of wood slows down and the
246 MLR decreases. From 200 s, a small increase in MLR occurs. To understand this
247 behavior, five thermocouples were inserted in CLT at 2, 10, 20, 30 and 38 mm
248 from the exposed surface. When the MLR increased, the thermocouple inserted at
249 10 mm from the surface reached a 100 ℃ plateau (not shown). This temperature is
250 assigned to water evolution and suggests that CLT undergoes dehydration reac-
251 tions [29]. At longer times (t > 200 s), the sample reaches a thermal steady state,
252 which is characterized by a quasi-constant MLR (Figure 3b) and a constant thick-
253 ness of char layer [30]. In a next step, a second peak of MLR occurs around
254 2500 s. At this peak, the temperature measured at 38 mm from the surface of
255 CLT is 320 ℃. It means that the pyrolysis front reaches the back of the sample
256 and thus the ceramic holder induces a thermal feedback (accumulation of heat)
257 that accelerates the decomposition [28]. Finally, flame extinguishes as the fuel con-
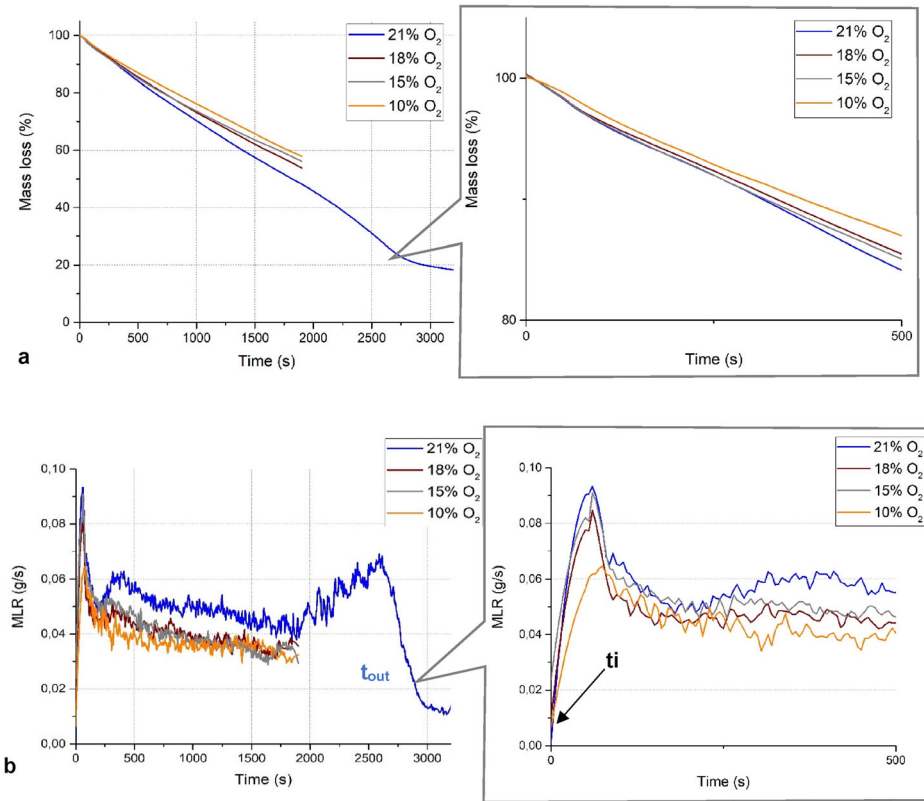
Figure 3. Effect of oxygen concentration on: (a) mass loss, (b) MLR.

tained in the solid phase diminishes and the MLR then decreases. Smoldering will then take place in the remaining char (visual observation).

Furthermore, the oxygen level affects the combustion process of CLT. Indeed, its decomposition occurs with flames at 21, 18 and 15 vol% O_2 but without flames at 10 vol% O_2. However, the MLR curves have all the same shape whatever the oxygen level (Figure 3b). The chemical reactions occurring in the condensed phase do not depend on the mass fraction of oxygen. Indeed, before 105 s, the mass loss curves and the peak of MLR (at ignition) at 21, 18 and 15 vol% O_2 (Figure 3a), (Table 2) are similar. This suggests that at the early stage of the test, the heat received at the surface of CLT mainly governs the decomposition of the sample. However, oxygen does modify the kinetics of decomposition, which are acceler- ated at high oxygen level. After 105 s, the mass loss of the specimen at 21 vol% O_2 accelerates while the mass losses at 18 and 15 vol% O_2 remain close with less than 0.7% of difference between them. Nevertheless, after 1100 s, the decomposi- tion becomes faster at 18 vol% O_2 (Figure 3a). Indeed, the decrease in oxygen level reduces the flame temperature and thus the flame thermal feedback to the surface of the solid [30]. Consequently, as less heat is transferred to the pyrolysis
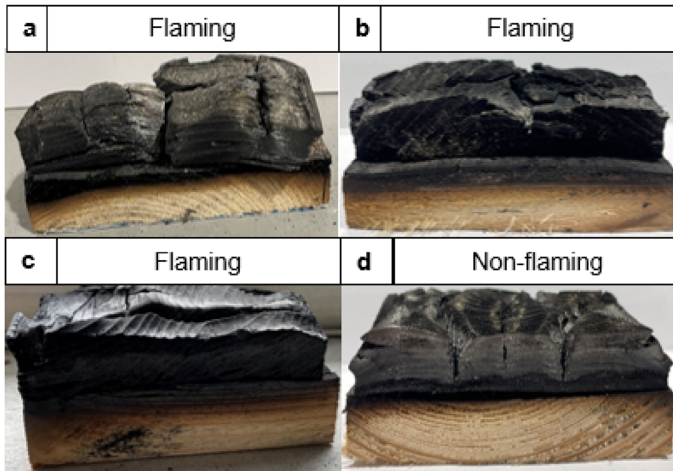
Effects of Oxygen Concentration on the Reaction to Fire of Cross-Laminated Timber

Table 2
Influence of Oxygen on the Fire Parameters at 50 kW/m^2

Oxygen level (%)	t_i (s)	pMLR (g/s)	pHRR (kW/m^2)
21	19	0.093	143
Standard error	1.5	0.004	12
18	18	0.085	138
Standard error	1.5	0.009	8
15	21	0.091	141
Standard error	0.7	0.010	9
10	–	0.065	41
Standard error		0.019	13

275 front with decreasing oxygen, the decomposition rate of wood is slower and the
276 amount of CLT residue after 32 min is 48% at 21 vol% O_2 vs. 56% at 15 vol%
277 O_2 (Figure 4) [27]. At 10 vol% O_2, the MLR curve has the same shape as other
278 oxygen levels but the decomposition occurs without flames. Though the heat flux
279 is high enough to decompose the sample into volatiles, there is not enough oxygen
280 for a flaming combustion to occur. Thus, the pMLR is decreased by 43% com-
281 pared to the pMLR at 21 vol% of O_2 (Table 2). As char is forming, the MLR
282 slows down and reaches a quasi-steady state.
283   In the condensed phase, the oxygen concentration affects the combustion pro-
284 cess (flaming or non-flaming) and the kinetics of decomposition. The higher the
285 oxygen content, the faster the mass loss is.

286 *3.1.1.2. Ignition and Heat Release* In the gas phase, depicted here by the oxygen
287 consumption based HRR, the reaction between the decomposition gases released
288 from wood and the ambient air occurs near the surface of the sample. The mix-
289 ture fuel/oxidant needs to reach the lean flammability limit to have a reaction of
290 combustion. If there is enough energy produced by the reaction to overcome heat
291 losses, the flame will spread on the whole surface of the sample [31]. For flaming
292 combustion experiments (21, 18 and 15 vol% O_2), their times to ignition (Table 2)
293 are not influenced by oxygen concentration as they are in the uncertainty range
294 ($\pm$ 3 s). Moreover, the HRR curves of flaming samples have all the same shape
295 (Figure 5). Indeed, the HRR increases rapidly to reach a peak and decreases after
296 as char forms. Then, the HRR curve reaches a steady state. As the pHRRs are in
297 the same range considering the standard errors of pHRRs at 21, 18 and 15% O_2
298 (Table 2), the oxygen concentration does not seem to have a significant influence.
299 The steady state reached after the peak is related to the thickness of the char layer
300 which is almost constant [31]. With the decrease of oxygen concentration, the
301 layer of char becomes thicker, involving less heat transferred to the pyrolysis
302 front. As a result, at the steady state, the higher the oxygen level is, the greater
303 the HRR is. Furthermore, at 15 vol% O_2, the weak concentration of oxygen indu-
304 ces a reduction in the flame intensity and thus the HRR decreases. At the end of
305 the test, small flames are located on the edges of the specimen.

Figure 4.   Sliced CLT after 32 min of test at 50 kW/m^2 at (a) 21% O$_2$, (b) 18% O$_2$, (c) 15% O$_2$ and (d) 10% O$_2$.
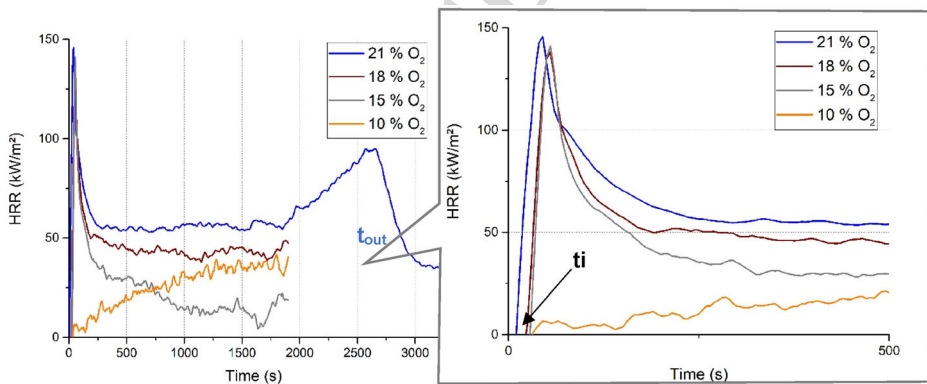
Figure 5.   Effect of oxygen concentration on the HRR.

306   From 15 to 10 vol% O$_2$, the combustion switches to flaming to non-flaming
307 mode (Figure 5). At 10 vol% O$_2$, the mixture fuel/oxidant remains below the
308 flammability limit because of the lack of oxygen. Thus, the HRR is low in the
309 early stage of the test but slowly increases next. Indeed, because of the heat
310 received at the surface of the char, smoldering occurs. The HRR remains then
311 steady at a level of 40 kW/m^2.
312   In summary, at 50 kW/m^2, two behaviors are observed according to the oxygen
313 concentration: flaming for 21%, 18% and 15% of oxygen and non-flaming for
314 10% of oxygen. The pMLR and times to ignition are not affected by oxygen
315 depletion in flaming combustion. Additionally, the oxygen concentration does not
316 affect the pHRRs values of flaming samples but it does influence the steady state
317 reached then.

318 *3.1.2. Gas Production* In addition to influencing the fire parameters of the CLT,
319 the oxygen level also has a strong influence on the gas production. The nature of
320 gaseous products and their quantities depend on the oxygen concentration.

321 Wood combustion is a multi-component complex process as it is composed of
322 three polymers: cellulose, hemicellulose and lignin. In general, thermal degradation
323 of wood starts with the evaporation of water by dehydration reactions. Then, dif-
324 ferent chemical bonds within the polymers are broken following either depolymer-
325 ization (breaking of the bonds between the monomer units of the wood polymers),
326 fragmentation (linkage of covalent bonds of polymers) and/or char formation.
327 This results in the release of volatile compounds and rearrangement reactions
328 within the wood matrix. Some of the volatiles produced are unstable and may
329 undergo secondary reactions, known as cracking (breaking of chemical bonds
330 within the volatile compounds) or recombination (combination of volatiles com-
331 pounds) [32].

332 More precisely, for the flaming specimens (21, 18 and 15 vol% O_2), many con-
333 densable organic compounds are identifiable on the FTIR spectra in the first
334 events of thermal exposure. The main compounds released are formaldehyde,
335 methanol, formic acid, acetic acid and phenol compounds. The detection of these
336 gases is in agreement with the literature [29, 32] (Table 3), which generally ascribe
337 their formation to fragmentation and/or breaking of chemical groups of wood
338 polymers. Besides, the oxygen level does not alter the detection of these organic
339 compounds nor the peak of release of formaldehyde in the early stage of the test
340 (Figure 6c). It suggests again that the first events in wood decomposition are
341 mainly depending on the heat level.

342 Then, as it blends with oxygen, this hot gaseous production oxidizes and igni-
343 tion occurs. Thus, the previous mentioned organics compounds are no more
344 detected on FTIR spectra while the production of CO_2 greatly increases. At igni-
345 tion, the CO_2 emission peaks around 30000 ppm for the three oxygen levels and
346 then reaches a steady state (Figure 6a). The high quantity of CO_2 released at igni-
347 tion is due to a rapid depolymerization of wood units that gives unstable interme-
348 diaries. These intermediaries contain carboxyl and carbonyl groups that undergo
349 fragmentation [32], for example:

$$HCOOH \rightarrow CO_2 + H_2 \text{ (decarboxylation of formic acid)}$$

351

$$O = CH_2 \rightarrow CO + H_2 \text{ (decarbonylation of formaldehyde).}$$
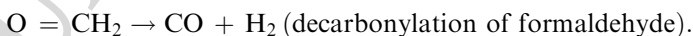
353 A small peak of CO, due to this depolymerization, is observed at ignition too
355 (Figure 6b) for all flaming specimens. However, at 15 vol% O_2 and from 750 s,
356 the CO production increases to reach a steady state and the organic species
357 observed at ignition as well as ethene are detected. Then, from 1700s and at both
358 18 and 15 vol% O_2, a peak in CO emission occurs. This increase may be related
359 to the lack of oxygen shifting the reaction of combustion towards incompleteness.
360 Indeed, as discussed previously, flames are less intense and located on the edges of
361 the specimen. The CO/CO_2 ratio is greater than 0.05, which means that the reac-

Table 3
Organic Compounds Detected in FTIR Analysis and Their Possible Way of Formation

Organic compound	Possible way of formation [32]
Formaldehyde (CH_2O)	Fragmentation of C–C bond linked to hydroxyl groups (lignin)
Methanol (CH_3OH)	Fragmentation of methoxy groups (hemicellulose and lignin)
Formic acid (HCOOH)	Rupture of carboxylic acid functions (hemicellulose)
Acetic acid (H_3CCOOH)	Fragmentation of acetic substituents (hemicellulose)
	Reaction of C–C bonds within and between alkyl chains (lignin)
	Breaking of glycosidic linkages (cellulose)
Phenol compounds	Breaking of ether bonds between monomers units (lignin)
	Reaction of C–C bonds within and between alkyl chains (lignin)

tion of combustion is incomplete. An increase in CH_4 (Figure 6e), which is released from demethylation reactions of the remaining methyl ($-CH_3$) substituents of the residue, occurs at the same time and thus argue in favor of the combustion reaction being below stoichiometry. The more methane is produced, the more aromatic the char is [32].

For the non-flaming specimen (10 vol% O_2), in the first events of thermal exposure, the same condensable organic compounds as flaming specimens are identifiable on the FTIR spectra (Table 3). However, as the low level of oxygen slows down the kinetics of decomposition and limit oxidation, additional gases such as acetaldehyde (C_2H_4O), methane and ethene (C_2H_4) are detected [25]. As a result, a high and broad peak of formaldehyde is produced at the beginning as well as one of acetaldehyde (Figure 6c and d). Acetaldehyde can be released from the thermal decomposition of levoglucosan ($C_6H_{10}O_5$), which is an intermediate compound released from cellulose decomposition [29]. Then, a strong and broad peak of CO production follows it while the CO_2 production is very low, with a CO/CO_2 ratio of 1.37. Indeed, there is not enough oxygen to oxidize the CO produced into CO_2. Thus, the production of unburnt hydrocarbon species is also promoted, with a high production of methane throughout the experiment (Figure 6e) while a peak of ethene (23 ppm) around 120 s is detected and is followed by a peak of propene (15 ppm).

For flaming specimens (21, 18 and 15 vol% O_2), oxygen decrease favors incomplete combustion at the end of the test with an increase in CO and CH_4 production. For non-flaming conditions, smoldering promotes the production of aldehydes (formaldehyde and acetaldehyde) and unburnt gases. Thus, the production of dangerous gases is favored at low oxygen level and when the combustion is non-flaming.

Effects of Oxygen Concentration on the Reaction to Fire of Cross-Laminated Timber
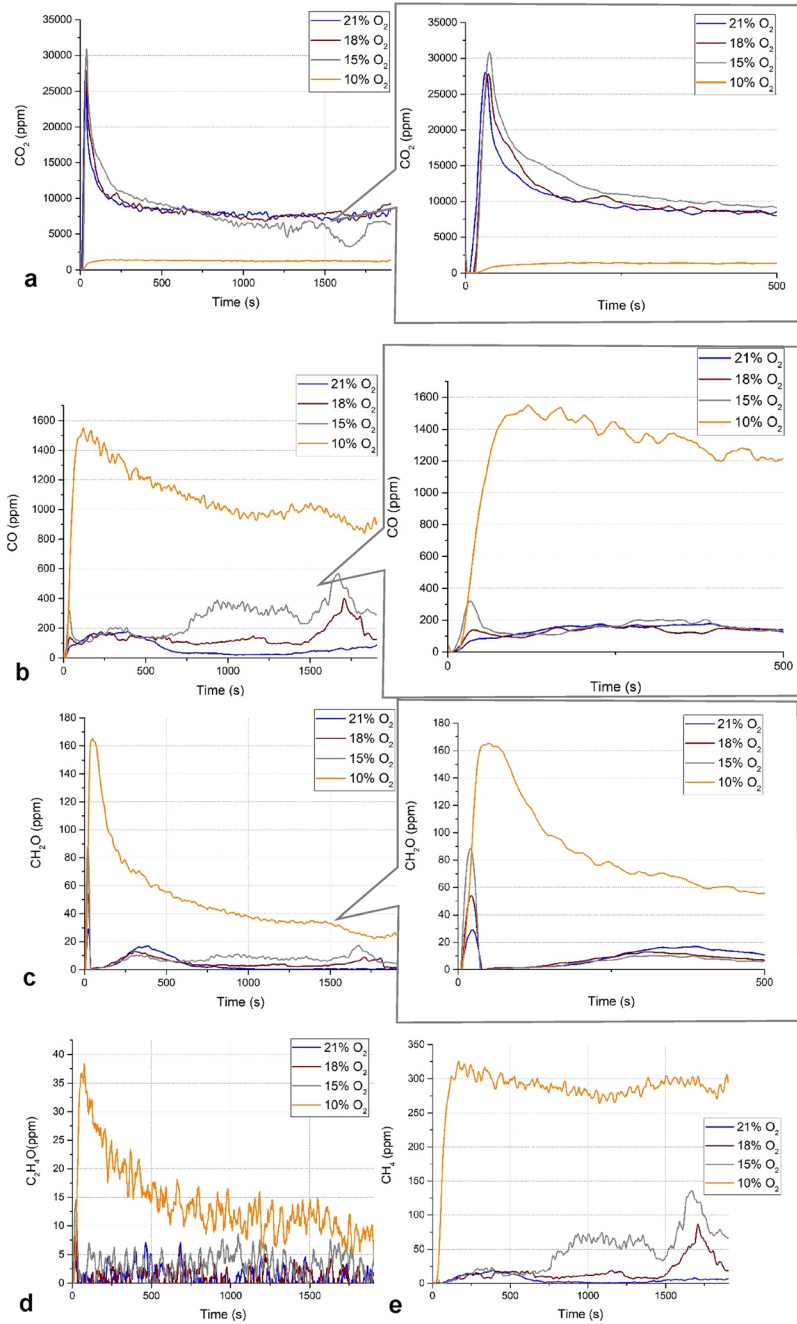
Figure 6. Influence of the oxygen level the gaseous emissions at 50 kW/m^2: (a) CO$_2$, (b) CO, (c) CH$_2$O, (d) C$_2$H$_4$O and (e) CH$_4$.

3.2. Aerosol Production

To complete the characterization of the gas phase, the influence of oxygen on the aerosol size distribution as well as the concentration of aerosol is now investigated.

At ignition, for the three burning samples (21, 18 and 15 vol% O_2), the distribution size is bimodal and centered on the modes 0.267 m and 0.109 m (Figure 7a). This corresponds to the accumulation mode of aerosols (0.1–1 m) which indicates the agglomeration and growth of particles [33]. The concentration of aerosols in these modes is the highest at 15 vol% O_2 but the orders of magnitude are close. Then, the bimodal distribution is crushed by a great increase in the mode 0.03 m (Figure 7b). Consequently, the distribution becomes monomodal and centered on the mode 0.03 m. This now corresponds to a nucleation mode (diameter inferior to 0.1 m) representing the formation of fresh aerosols. This may be due to the nucleation of volatiles particles as the effluent mixture cools down after ignition. Indeed, vaporized gases condensed and became particles having very small size [33], [36, 37]. Globally, the concentration in this mode is of the same magnitude at 21, 18 and 15 vol% O_2.

For 10 vol% O_2, the combustion is non-flaming and the distribution is monomodal centered on the mode 0.03 m (Figure 7a). Compared to the flaming specimens, the concentration in the mode 0.03 m at 10 vol% O_2 is slightly higher (Figure 7b). In some studies, the lack of oxygen is shown to increase the number of particles. Indeed, with less oxygen available, the number of unburnt particles increases [36, 37].

For the flaming specimens, a bimodal distribution centered on the modes 0.267 m and 0.109 m is observed at ignition. Then, it is replaced by a monomodal distribution centered on the mode 0.03 m. For the non-flaming specimen, the distribution is monomodal centered on the mode 0.03 m. Globally, the distribution in size of aerosols is not influenced by oxygen level but by the combustion process.

The influence of oxygen on the reaction to fire, the gas and the aerosol production of CLT was fully assessed at 50 kW/m². To verify if similar behaviors are observed, it is crucial to study the influence of oxygen on less aggressive fire scenarios.

3.3. Influence of Oxygen Level at 20 kW/m²

The reaction to fire of CLT is also strongly dependent on the thermal attack, thus the influence of the heat flux was evaluated at 20 kW/m². This thermal attack enables to study less aggressive fire scenarios, such as smoldering, with slower decomposition kinetics.

3.3.1. Mass Loss and Heat Release 3.3.1.1. Mass Loss The evolutions of remaining mass as a function of time (Figure 9a) are very slow and similar at the beginning of the thermal exposure whatever the oxygen concentration. However, around 550 s for 21 vol% O_2, and around 1042 s for 18 vol% O_2, the samples ignite and the mass fraction of CLT drops while the MLR reaches a peak (Fig-
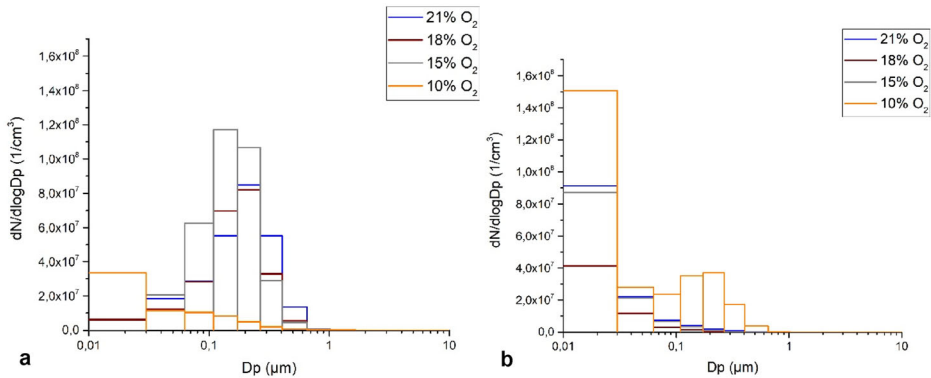
Figure 7. Distribution size of aerosols at 50 kW/m^2 at: (a) ti, (b) 1484 s.

431 ure 9b). The time to reach the peak of MLR more than doubles between 21 and
432 18 vol% O_2 and the pMLR is the highest for 21 vol% O_2 (Table 4). The lack of
433 oxygen delays the ignition [38, 39] as well as the flame's temperature [40], which
434 reduces the solid degradation rate. In the end, the samples flame out to reach a
435 steady state around 0.25 g/s. Furthermore, the amount of CLT residue after
436 32 min is 68% at 21 vol% O_2 whereas it is 77% at 18 vol% O_2. The pyrolysis
437 front has reached higher thickness at 21 vol% O_2 than at 18 vol% O_2 as the char
438 formed is less protective (Figure 8).

439 At 15 and 10 of oxygen, the decomposition occurs without flames. The mass
440 losses (Figure 9a) are similar until 700 s where the decomposition rate at 15% O_2
441 slightly increases. As a result, the MLRs follow a slow increase in the beginning,
442 as water evaporates, and tend to be constant for the rest of the test (Figure 9b).
443 The amount of CLT residue after 32 min is 81% at 15 vol% O_2 and 82% at 10
444 vol% O_2 (Figure 8c and d). At these low concentrations and under 20 kW/m^2, the
445 influence of oxygen does not seem to have a significant impact on the decomposi-
446 tion of the CLT.

447 In the condensed phase, as at 50 kW/m^2, the oxygen concentration affects the
448 combustion process (flaming or non-flaming) and the kinetics of decomposition.
449 The higher the oxygen content is the faster the mass loss is.

450 *3.3.1.2. Ignition and Heat Release* In the gas phase, the HRR curves depict two
451 combustion behaviors (Figure 10). Indeed, at 21% and 18% of oxygen, a peak of
452 heat release from flaming combustion is observed while at 15% and 10% of oxy-
453 gen the non-flaming decomposition is depicted by a slow and low increase in
454 HRR. For flaming samples, the peak of HRR is reduced of 48% between the
455 peak of HRR at 21% O_2 and the peak of HRR at 18% O_2. This is due to the low
456 oxygen amount that does not allow a complete reaction neither a high tempera-
457 ture of flame. After ignition, both samples rapidly flame out. For lower oxygen
458 levels, the HRR increases slowly to reach a steady state around 20 kW/m^2. As the
459 behaviors are similar, the influence of oxygen seems again negligible.

Table 4
**Influence of Oxygen on the Fire Parameters at 20 kW/m^2**

Oxygen level (%)	t_i (s)	pMLR (g/s)	pHRR (kW/m^2)
21	400	0.061	96
Standard error	105	0.003	4
18	1042	0.041	51
Standard error	257	0.021	29
15	–	0.023	20
Standard error		0.034	4
10	–	0.024	22
Standard error		0.022	13
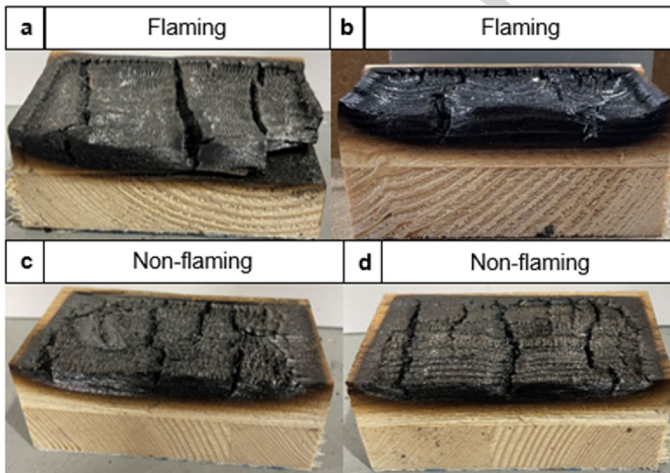
Figure 8.   Sliced CLT after 32 min of test at 20 kW/m^2 at (a) 21% O$_2$, (b) 18% O$_2$, (c) 15% O$_2$ and (d) 10% O$_2$.

In summary, at 20 kW/m^2, two behaviors are observed according to the oxygen concentration: flaming for 21% and 18% O_2 and non-flaming for 15% and 10% O_2. The mass loss and heat release rates are similar whatever the oxygen level when the combustion is non-flaming. For flaming combustion, the ignition is delayed and less intense with oxygen decrease.

3.3.2. Gas Production For the flaming specimens (21 vol% O_2 and 18 vol% O_2), in the first events of thermal decomposition, CLT released ethene and the same organic compounds as it did at 50 kW/m^2, namely formaldehyde, methanol, formic acid, acetic acid and phenol compounds (Table 3). At 21 vol% O_2, before 200 s, a peak of formaldehyde occurs (Figure 11c). Then, at 21 vol% O_2 and from 300 s, another peak of formaldehyde is reached as well as one of CO and CH_4 (Figure 11b and d). At 400 s, the sample ignites and a peak in CO_2 occurs (Fig-

Effects of Oxygen Concentration on the Reaction to Fire of Cross-Laminated Timber
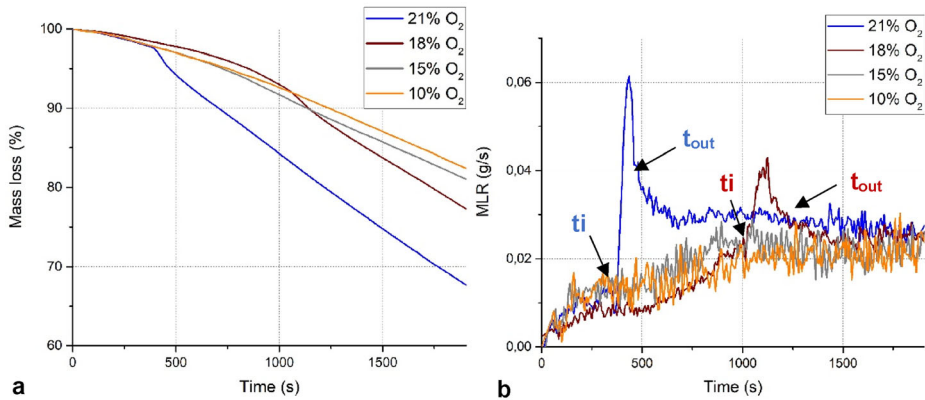
Figure 9.   Effect of oxygen concentration on: (a) the mass loss, (b) the MLR.
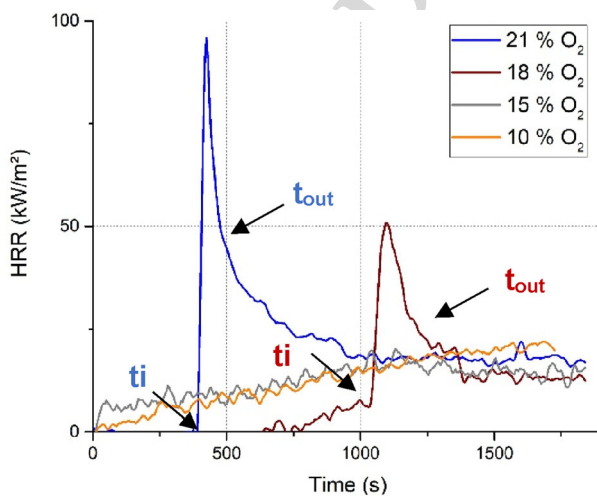
Figure 10.   Effect of oxygen concentration on the HRR.

472   ure 11a). The CO_2 concentration rapidly decreases until the sample flames out. As
473   a result, peaks of CH_2O, CO and CH_4 arise at 1050 s. The behavior is similar at
474   18 vol% O_2 but it is delayed in time. Indeed, the second peak of formaldehyde
475   (Figure 11c) as well as these of CO and CH_4 are reached at 1035 s (Figure 11b
476   and d). CLT ignites at 1042 s with a peak of CO_2 emission and then flames out at
477   1160 s with an increase in CH_2O, CO and CH_4. At the end of the test, the pro-
478   duction of gases at 18 vol% O_2 reaches a steady state instead of decreasing as at
479   21 vol% O_2. In general, for both conditions, the CO/CO_2 is greater than 0.05 dur-
480   ing the whole test (incomplete combustion). Moreover, the production of carbon
481   dioxide is slightly higher at 21 vol% O_2 than at 18 vol% O_2 while it is the oppo-
482   site for carbon monoxide and methane production.
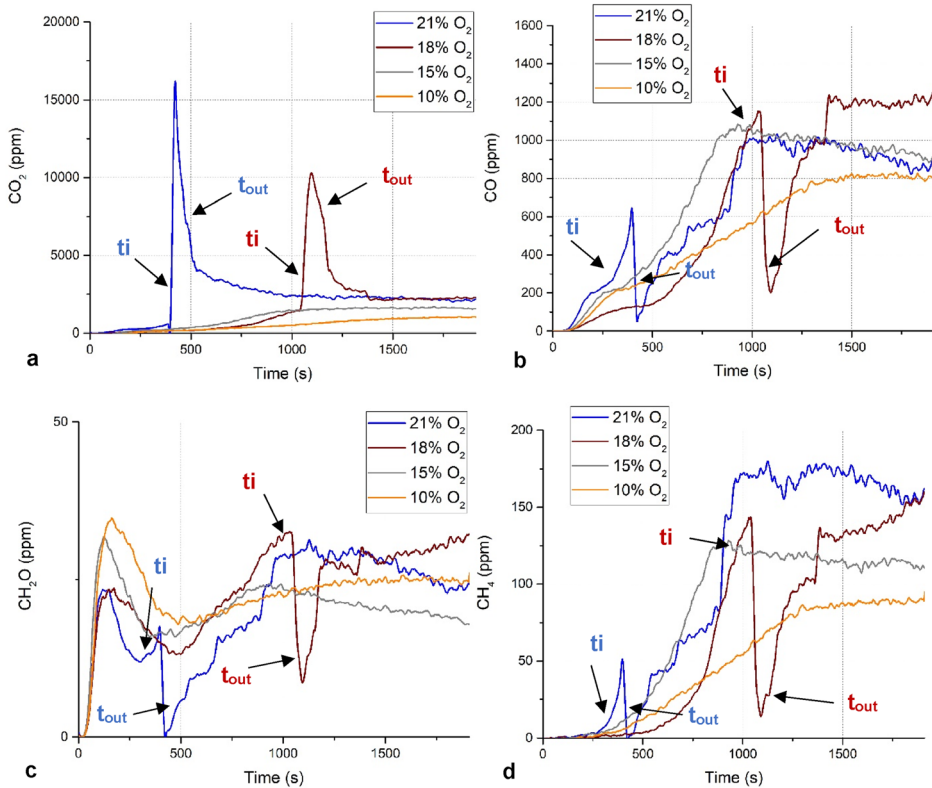
Figure 11. Influence of the oxygen level the gaseous emissions at 20 kW/m^2: (a) CO$_2$, (b) CO, (c) CH$_2$O and (d) CH$_4$.

For non-flaming combustion (15% and 10% O$_2$), FTIR spectra reveal that the organic compounds produced are the same as for the flaming specimens and that they are produced during the whole test. For both oxygen levels, the CO/CO$_2$ ratio is greater than 0.05 during the whole test as the production of CO$_2$ is very low (Figure 11a). At the beginning of the test, before 250 s, a peak of formaldehyde comes up (Figure 11c) as wood decomposes and then the production drops down. In the meantime, the production in CO and CH$_4$ significantly increases, as wood is carbonizing, and they reach a maximum at 935 s at 15 vol% O$_2$ and 1500 s at 10 vol% O$_2$. It slightly decreases after (Figure 11a and d) and an increase in formaldehyde is also observed at these times. The same behaviors are observed at 15 vol% O$_2$ and 10 vol% O$_2$, but again the phenomena are delayed in time with oxygen decrease. For non-flaming conditions, the production of CO and CH$_4$ is promoted with the increase of oxygen concentration.

For flaming specimens, oxygen decrease favors incomplete combustion with higher production of CO and CH$_4$. However, for non-flaming conditions, the higher the oxygen level is the higher the production of CO and CH$_4$ is.

499   *3.3.3. Aerosol Production* At ignition, for the burning samples at 21% O_2 and
500   18% O_2, the distribution is bimodal and centered on the modes 0.267 m and
501   0.109 m (Figure 12a), which corresponds to the accumulation mode. Then, as for
502   50 kW/m^2, the bimodal distribution is crushed by a great increase in the mode
503   0.03 m. Consequently, the distribution becomes monomodal and centered on the
504   mode 0.03 m (Figure 12b). This corresponds again to the nucleation mode. The
505   concentration in aerosols is slightly higher at 21% O_2 but globally of the same
506   magnitude.
507   For the non-flaming specimens, the distribution is also monomodal centered on
508   the mode 0.03 m during the whole test (Figure 12a and b). The concentration in
509   the mode 0.03 m is similar between 15 and 10% O_2. However, it is slightly
510   reduced compared to 21 and 18% O_2 samples. It can be due to the change in the
511   combustion process, here smoldering which induces slower decomposition rates
512   [34].
513   For the flaming specimen, a bimodal distribution centered on the modes
514   0.267 m and 0.109 m is observed at ignition at 21% O_2 and at 18%. Then, it is
515   replaced by a monomodal distribution centered on 0.03 m. For the non-flaming
516   specimen, the distribution is monomodal centered on the mode 0.03 m.

3.4. General Discussion

518   The fire behavior as well as the gas and aerosol production of CLT according to
519   the oxygen concentration and the heat flux was investigated. These latter parame-
520   ters are limiting factors to enable combustion as well as altering the kinetics of
521   decomposition. The combination of both of them highlights different fire scenarios
522   where the quantity of gases produced can be potentially toxic.
523   The first type of decomposition scenario obtained with CLT is flaming combus-
524   tion (Figure 15). At 50 kW/m^2, the oxygen level is not high enough to disturb the
525   combustion regime in the early stage of the test and the condensed phase is not
526   affected. Indeed, the times to ignition (Table 2) and the maxima of MLR are simi-
527   lar at 21, 18 and 15 vol% O_2 (Figure 13). It could be assumed that the surface
528   oxidation reactions would contribute to the thermal decomposition of CLT but Di
529   Blasi [41] claims that the flame prevents the char oxidation. Oxygen cannot diffuse
530   through the flame as it is consumed at its boundaries. Moreover, according to
531   Kashiwagi [42], the region near the flame is poor in oxygen because of the
532   homogenous reactions of combustion. As a result, all oxidative reactions near the
533   surface stop. These observations are in accordance with the fact that oxygen diffu-
534   sion to the surface of CLT is limited by the increased mass heat flux of gaseous
535   products over time. As a result, the heterogeneous reactions of the solid phase
536   cannot occur once the flame is established. However, the oxygen concentration
537   does affect the gas phase. With oxygen decrease, the flaming combustion shifts in
538   time to incompleteness with higher CO and CH_4 yields (Figure 14). The oxidation
539   reactions of organic compounds into CO_2 are disadvantaged against oxidation
540   into CO as well as demethylation at low oxygen levels. It should be noted that
541   although the combustion regime is slightly altered with oxygen decrease, the yields
542   in CO_2 are marginally affected. Furthermore, lowering the heat flux to 20 kW/m^2
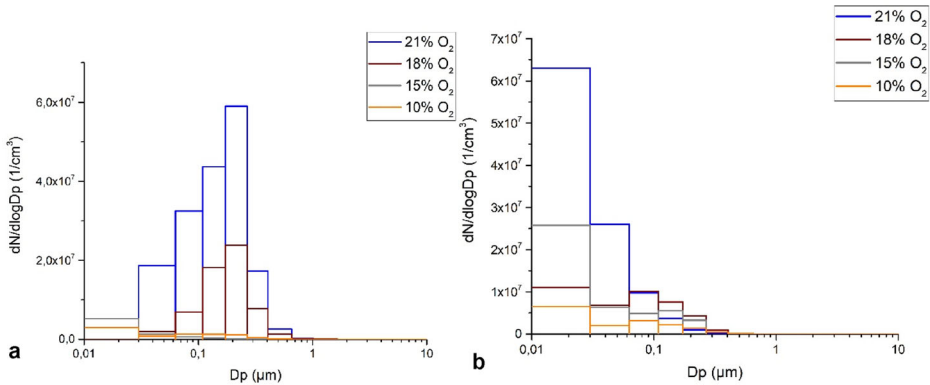
Figure 12. **Distribution size of aerosols at 20 kW/m² at: (a) ti, (b) 1484 s.**
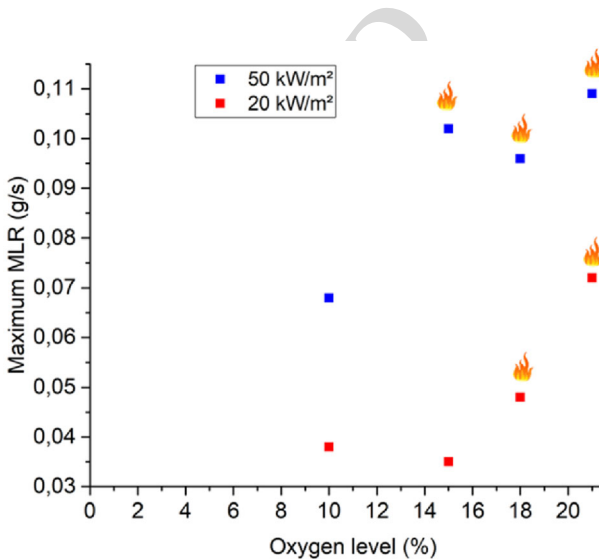
Figure 13. **Effect of oxygen and heat flux on the maximum MLR.**

leads to slower kinetics of decomposition (20 kW/m², 21 vol% O_2 and 20 kW/m², 18 vol% O_2). As less heat is received at the surface of CLT, the ignition process is both governed by heat and oxygen concentration. At 21 vol% O_2, the ignition of CLT is 22 times delayed in time compared to 50 kW/m². Similarly, at 20 kW/m², the time to ignition at 18 vol% O_2 is increased by a factor of 2.5 compared to the time to ignition at 18 vol% O_2. Moreover, the pMLRs are greatly lowered compared to 50 kW/m² (Figure 13). Between 50 and 20 kW/m², the pMLRs are reduced by 34% at 21 vol% O_2 and of 50% at 18 vol% O_2. Consequently, the wood matrix has time to rearrange into a more stable matrix. Indeed, before a bond can be completely broken from the wood matrix, new bonds could form to

Effects of Oxygen Concentration on the Reaction to Fire of Cross-Laminated Timber
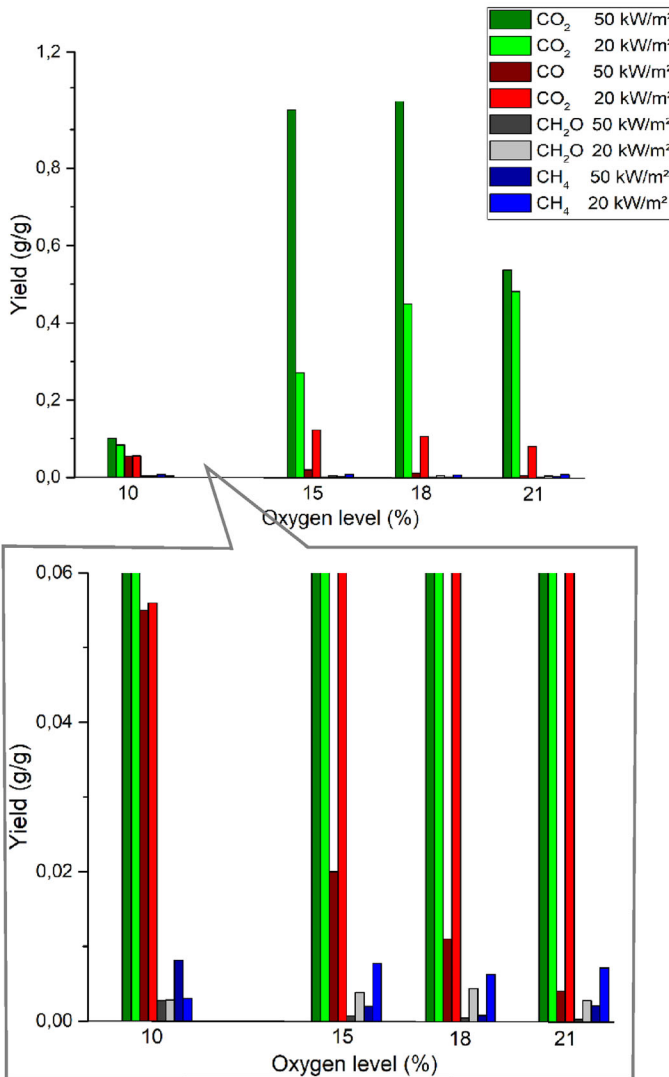
Figure 14. Total yields of CO2, CO, CH2O and CH4 as a function of oxygen level and heat flux.

553 bond the fragment back to the previous wood matrix [43]. Thus, less organic vola-
554 tiles are produced while the yields of CO and CH_4 are promoted (Figure 14). As
555 CLT rapidly flames out, a dramatic increase in CO and CH_4 occurs, which is
556 amplified with oxygen decrease. For all types of flaming scenarios described, the
557 distribution of aerosol particle size is centered on the modes 0.267 and 0.109 m at
558 ignition and then it shifts to the mode 0.03 m. Increasing the heat flux increases
559 the number of particles per cm^3, which is a risk as submicronic particles can pene-
560 trate the lungs [37].

561   The second type of decomposition scenario of CLT is non-flaming combustion
562   (Figure 15). The oxygen vitiation affects the combustion process. Indeed, at
563   50 kW/m^2, though the MLR curve at 10 vol% fits the shape of the flaming speci-
564   men (21, 18 and 15 vol% O_2) (Figure 3a), there is not enough oxygen to ignite the
565   released volatiles and only smoldering occurs. However, it should be highlighted
566   that below 21 vol% O_2 at 50 kW/m^2, the MLR curves of flaming and non-flaming
567   specimens are close in value (around 0.4 g/s) during the steady state reached after
568   the peak. This again suggests that the heat flux mainly governs the decomposition
569   process and that oxygen has a low impact on it. It is also interesting to note that
570   the pMLR reached at 10 vol% O_2 is similar to that at 21 vol% O_2 at 20 kW/m^2
571   (at ignition) (Figure 13). It confirms the limiting role of oxygen in the combustion
572   regime. Moreover, the lack of oxygen increases the production of C_2H_4O (Fig-
573   ure 6d) and the yields of CH_4 and CO as there is not enough oxygen to oxidize
574   organic volatiles into CO_2 (Figure 14). At high heat flux, non-flaming combustion
575   is a threat to fire safety as the production of unburnt gases is promoted and the
576   decomposition and heat release rates remain high. Moreover, the production of
577   aerosols is significant which is all the more dangerous as the distribution size of
578   aerosols is centered on the mode 0.03 m (lung penetration). Reducing the heat
579   flux to 20 kW/m^2 leads to a higher demand in oxygen to have a flaming combus-
580   tion. Indeed, the combustion is not flaming at 15 vol% O_2 whereas it was flaming
581   at 50 kW/m^2. The low heat received at the CLT surface also results in lower
582   decomposition rates as the pMLR is reduced by 63% between the 10 vol% O_2
583   cases (Figure 13). It should be underlined that the pMLR at 15 and 10 vol% O_2
584   are similar (Figure 13). Thus, the oxygen has no significant impact on the decom-
585   position of the condensed phase. Moreover, the yields of CO_2 and CO are similar
586   at 10 vol% O_2 between 50 and 20 kW/m^2 while those of CH_4 are slightly higher
587   at 50 kW/m^2 (Figure 14). This highlights the low impact of the heat flux on gas
588   production when the combustion is not flaming. Finally, for non-flaming combus-
589   tions, the distribution of particle size is also centered on the mode 0.03 m but with
590   a lower concentration than for flaming conditions.

4. Conclusion

592   The assessment of the fire behavior, the gas production and the aerosol size distri-
593   bution of Cross-Laminated Timber were carried out with a homemade (based on
594   the ISO 5660–5 standard) Controlled-Atmosphere Cone Calorimeter coupled with
595   a FTIR and an ELPI. This is an appropriate approach to examine the effect of
596   the oxygen and the irradiance level on the solid/gas phase phenomena occurring
597   during the thermal degradation of CLT. Both heat flux and oxygen are revealed
598   to be limiting factors in the combustion process, which enables the classification
599   of fire behaviors of CLT (Figure 16).
600   In general, oxygen vitiation shifted the reaction of combustion towards incom-
601   pleteness or even prevented it in some cases. It also greatly promoted the emission
602   of unburnt species such as carbon monoxide and methane. These phenomena are
603   favored at reduced heat flux. For all flaming specimens, the aerosol size distribu-

Effects of Oxygen Concentration on the Reaction to Fire of Cross-Laminated Timber
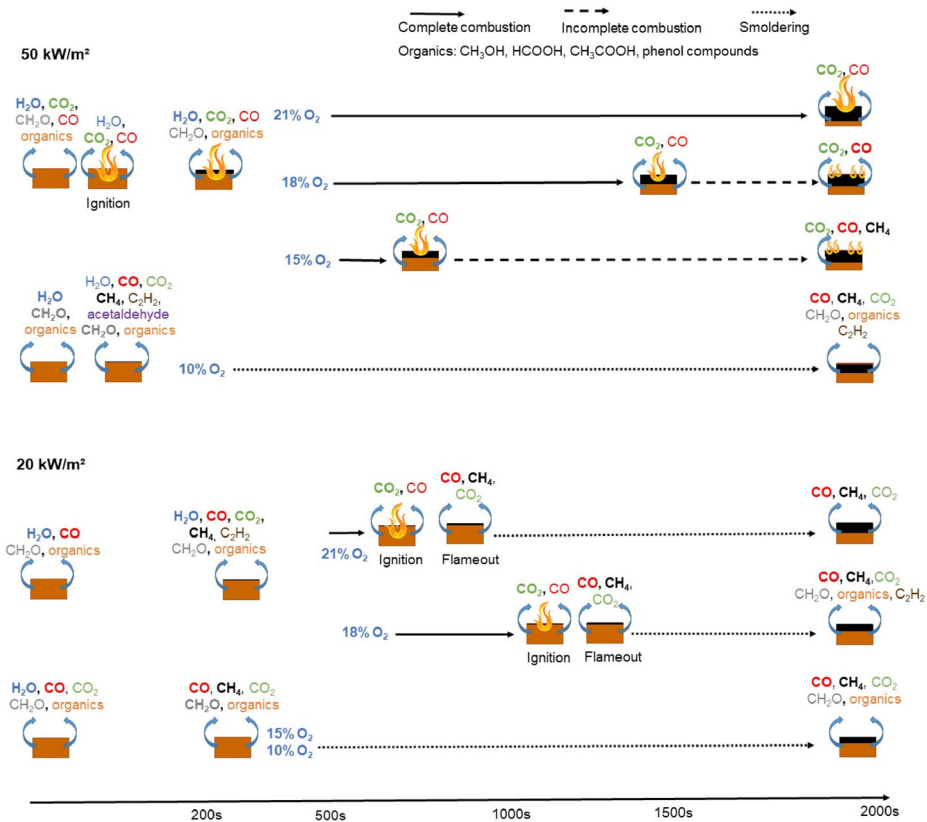
Figure 15. Flaming and non-flaming decomposition of CLT.
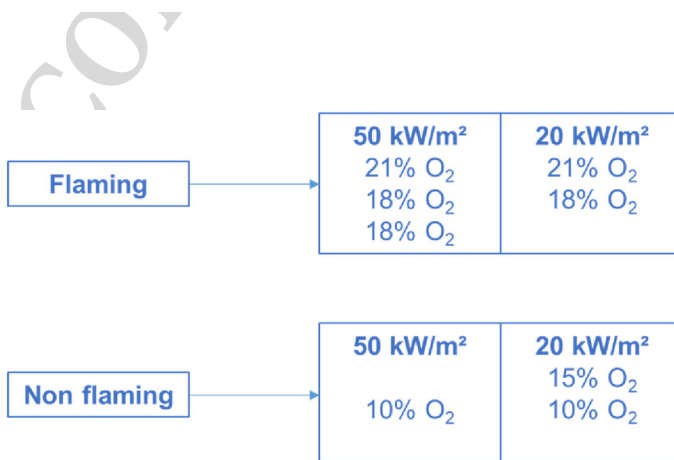
Figure 16. Classification of fire behavior of CLT according to oxygen level and heat flux.

604 tion is centered on the modes 0.267 m and 0.109 m at ignition and then shifts to
605 the mode 0.03 m, while for non-flaming specimens the distribution size of aerosols
606 is centered on the mode 0.03 m.

607   This study highlights the hazards of different fire scenarios. CLT exposed to a
608 high heat flux combined with low oxygen level creates an environment with a sig-
609 nificant amount of dangerous gases and submicronic aerosols. Besides, smoldering
610 is a hazard for fire spread in a room. Further investigations on the lower flamma-
611 bility limit of CLT according to oxygen level and heat flux would be interesting to
612 have a finer understanding of its behavior. A finer measuring range of the distri-
613 bution size of aerosols could be also beneficial to better assess the aerosol produc-
614 tion.

Funding

References

619   1. Hall JJ, Harwood B (1995) Smoke or burns - Which is deadlier ?. NFPA J 89(1):38–43
620   2. Guillaume E, Effets du feu sur les personnes, p 163
621   3. ISO 13571 (2012) Life-threatening components of fire—Guidelines for the estimation of
622   time to compromised tenability in fires
623   4. ISO 5660–1:2015 (2015) Reaction-to-fire tests—Heat release, smoke production and
624   mass loss rate—Part 1: heat release rate (cone calorimeter method) and smoke produc-
625   tion rate (dynamic measurement)
626   5. Werrel M, Deubel JH, Krüger S, Hofmann A, Krause U (2014) The calculation of the
627   heat release rate by oxygen consumption in a controlled-atmosphere cone calorimeter:
628   heat release rate in a controlled-atmosphere cone calorimeter. Fire Mater 385(2):204–
629   226. 10.1002/fam.2175
630   6. Marquis D, Guillaume E, Lesenechal D (2013) Accuracy (Trueness and Precision) of
631   cone calorimeter tests with and without a vitiated air enclosure. Procedia Eng 62:103–
632   119. 10.1016/j.proeng.2013.08.048
633   7. Mulholland G, Janssens M, Yusa S, Twilley W, Babrauskas V (1991) The effect of oxy-
634   gen concentration on Co and smoke produced by flames. Fire Saf Sci 3:585–594.
635   10.3801/IAFSS.FSS.3-585
636   8. Nelson GL (1995) Fire and Polymers II: Materials and Tests for Hazard Prevention, in
637   ACS Symposium Series. American Chemical Society, Washington, DC
638   9. Marquis D, Guillaume E, Camillo A (2014) Effects of oxygen availability on the com-
639   bustion behaviour of materials in a controlled atmosphere cone calorimeter. Fire Saf
640   Sci 11:138–151. 10.3801/IAFSS.FSS.11-138
641 10. Sarah C (2019) An instrumented controlled-atmosphere cone calorimeter to characterize
642   electrical cable behavior in depleted fires, p 249
643 11. Etienne M, Evaluation du risque d'inflammation de gaz imbrûlés au cours d'un incendie
644   en milieu sous-ventilé, p 283
645 12. Marquis DM, Guillaume E, Effects of under-ventilated conditions on the reaction-to-
646   fire of a polyisocyanurate foam, p 13

Journal : **10694_FIRE**	Dispatch : **19-12-2023** Pages : **26**
	□ LE ☑ TYPESET
MS NO : **1518**	☑ CP ☑ DISK

Effects of Oxygen Concentration on the Reaction to Fire of Cross-Laminated Timber

647 13. Hermouet F, Développement d'une approche innovante de modélisation de la cinétique
648   de décomposition thermique des matériaux solides en espaces confinés sous-ventilés.
649   sApplication aux incendies en tunnel, p 265
650 14 Swann JD, Ding Y, McKinnon MB, Stoliarov SI (2017) Controlled atmosphere pyroly-
651   sis apparatus II (CAPA II): a new tool for analysis of pyrolysis of charring and intumes-
652   cent polymers. Fire Saf J 91:130–139. 10.1016/j.firesaf.2017.03.038
653 15. Marquis DM, Guillaume E, Camillo A, Rogaume T, Usage of controlled-atmosphere
654   cone calorimeter to provide input data for toxicity modelling, p 13
655 16. Mustafa BG, Toxic species and particulate emissions from wood and pool fires, p 342
656 17. ISO/TS 5660–5:2020 (2020) Reaction-to-fire tests—Heat release, smoke production and
657   mass loss rate—Part 5: heat release rate (cone calorimeter method) and smoke produc-
658   tion rate (dynamic measurement) under reduced oxygen atmospheres
659 18 Tewarson A, Jiang F, Morikawa T (1993) Ventilation-controlled combustion of poly-
660   mers. Combust Flame 95(1–2):151–169. 10.1016/0010-2180(93)90058-B
661 19 Brohez S, Marlair G, Delvosalle C (2008) The effect of oxygen concentration on CO
662   and soot yields in fires. Fire Mater 32(3):141–158. 10.1002/fam.960
663 20. EN 13238:2010 (2010) Reaction to fire tests for building products - Conditioning proce-
664   dures and general rules for selection of substrates
665 21. Alarifi A, Andrews G, Witty L, Phylaktou H (2013) Ignition and toxicity of selected
666   aircraft interior materials using the cone calorimeter and FTIR analysis, Proceedings of
667   the InterFlam 2013. InterScience Communications: London, UK. 1: 37–48, ISBN: 978-
668   0-9556548-9-3
669 22. Irshad A, Andrews G, Phylaktou H, Gibbs B (2019) International seminar on fire and
670   explosion hazards (9; 2019; Saint Petersburg, Russia). Develop Control Atmos Cone
671   Calorim Simulate Compart Fires . 10.18720/SPBPU/2/K19-90
672 23. Ngohang FE, Combination of mass loss cone, Fourier transform infrared spectroscopy
673   and electrical low pressure impactor to extend fire behaviour characterization of materi-
674   als, p 155
675 24. ISO 19706:2011 (2011) Guidelines for assessing the fire threat to people
676 25 Stec AA, Hull R (2010) Fire Toxicity. Woodhead Publishing, Sawston
677 26. Friquin KL (2011) Material properties and external factors influencing the charring rate
678   of solid wood and glue-laminated timber. Fire Mater 325(5):303–327. 10.1002/fam.1055
679 27 Di Blasi C, Hernandez HG, Santoro A (2000) Radiative Pyrolysis of Single Moist Wood
680   Particles. American Chemical Society, Washington, DC
681 28. Quintiere JG, Rhodes B (1994) Fire growth models for materials, National Institute of
682   Standards and Technology
683 29 Sullivan AL, Ball R (2012) Thermal decomposition and combustion chemistry of cellu-
684   losic biomass. Atmos Environ 47:133–141. 10.1016/j.atmosenv.2011.11.022
685 30 Cuevas J, Torero JL, Maluk C (2021) Flame extinction and burning behaviour of timber
686   under varied oxygen concentrations. Fire Saf J 120:103087. 10.1016/j.firesaf.2020.103087
687 31. Mikkola E (1991) Charring of wood based materials. Fire Saf Sci 3:547–556. 10.3801/
688   IAFSS.FSS.3-547
689 32 Collard F-X, Blin J (2014) A review on pyrolysis of biomass constituents: mechanisms
690   and composition of the products obtained from the conversion of cellulose, hemicellu-
691   loses and lignin. Renew Sustain Energy Rev 38:594–608. 10.1016/j.rser.2014.06.013
692 33 Laaongnaun S, Patumsawad S (2022) Particulate matter characterization of the combus-
693   tion emissions from agricultural waste products. Heliyon 8(8):e10392. 10.1016/j.heli-
694   yon.2022.e10392
695 34. Hosseini S et al (2010) Particle size distributions from laboratory-scale biomass fires
696   using fast response instruments. Atmos Chem Phys 10(16):8065–8076

35 Lighty JS, Veranth JM, Sarofim AF (2000) Combustion aerosols: factors governing their size and composition and implications to human health. J Air Waste Manag Assoc 50 (9):1565–1618. 10.1080/10473289.2000.10464197

36 Hertzberg T, Blomqvist P (2003) Particles from fires: a screening of common materials found in buildings. Fire Mater 27(6):295–314. 10.1002/fam.837

37. Nussbaumer T, Czasch C, Klippel N, Johansson L, Tullin C 9, Particulate Emissions from Biomass Combustion in IEA Countries. p 40

38 Hurley MJ et al (2016) SFPE Handbook of Fire Protection Engineering. Springer, New York. 10.1007/978-1-4939-2565-0

39 Delichatsios MA (2005) Piloted ignition times, critical heat fluxes and mass loss rates at reduced oxygen atmospheres. Fire Saf J 40(3):197–212. 10.1016/j.firesaf.2004.11.005

40 Ohlemiller TJ, Kashiwagi T, Werner K (1987) Wood gasification at fire level heat fluxes. Combust Flame 69(2):155–170. 10.1016/0010-2180(87)90028-9

41. Di Blasi C (2004) The burning of plastics. In: Troitzsch J (ed) Plastics Flammability Handbook, Principles Regulation Testing and Approval Carl Hanser Verlag GmbH & Co KG, München, pp 47–132

42 Kashiwagi T (1994) Polymer combustion and flammability—Role of the condensed phase. Symp (Int) Combust 25(1):1423–1437. 10.1016/S0082-0784(06)80786-1

43 Shen J, Wang X-S, Garcia-Perez M, Mourant D, Rhodes MJ, Li C-Z (2009) Effects of particle size on the fast pyrolysis of oil mallee woody biomass. Fuel 88(10):1810–1817. 10.1016/j.fuel.2009.05.001